Fuel 320 (2022) 123869

Contents lists available at ScienceDirect

Fuel

journal homepage: www.elsevier.com/locate/fuel

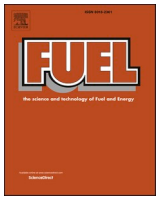

Full Length Article

Tyre pyrolytic oil fuel blends in a modern compression ignition engine: A comprehensive combustion and emissions analysis

Maciej Mikulski [a,*], Jacek Hunicz [b], Kamil Duda [c], Paweł Kazimierski [d], Tomasz Suchocki [d], Arkadiusz Rybak [b]

[a] University of Vaasa, School of Technology and Innovation, Wolffintie 34, FI-65200 Vaasa, Finland
[b] Lublin University of Technology, Faculty of Mechanical Engineering, Nadbystrzycka 36, 20-618 Lublin, Poland
[c] University of Warmia and Mazury, Faculty of Technical Sciences, Słoneczna 46 A, 10-710 Olsztyn, Poland
[d] Polish Academy of Sciences, Institute of Fluid Flow Machinery, Generala Jozefa Fiszera 14, 80-231, Gdansk, Poland

ARTICLE INFO

Keywords:
Tyres
Pyrolysis
Fuel characterisation
Compression ignition engine
Emissions
EPA Tier 4

ABSTRACT

There is abundant worldwide research into combustion engine applications for tyre pyrolysis oil (TPO). However, most studies are methodologically outdated in terms of their assumed technology, either with regard to TPO production or engine application, or in their analytical approaches. The variety of radically different studies produce conflicting or ambiguous results, rendering TPÓs role as a feasible future fuel uncertain. This study is the first to provide state-of-the art combustion analysis results for thoroughly-evaluated TPO fraction optimised in a modern, industry-grade pyrolytic reactor. The fuel blends are selected for engine tests, taking into account the overall availability/compatibility of their TPO fractions with diesel. Testing with a modern, sophisticated single-cylinder research engine provides detailed analysis of combustion and both regulated and unregulated emissions. Emissions results are supported by FTIR analysis of exhaust gases, including identification of 23 species. The results show that contemporary Tier 4-compliant combustion systems with multi-pulse injection can handle high TPO-content fuels without needing re-calibration. With diesel/TPO blends of up to 40% TPO admixture, combustion phasing is substantially delayed (by 3CAD) only at near-idle loads and particularly when using heavy exhaust gas recirculation. The consequential differences in performance and emissions diminish over the test cycle. Current US EPA Tier 4 emission limits are not particularly challenging for TPO, even at 40% blending rate, but its elevated levels of particulate matter (25% increase over test cycle versus diesel baseline), sulphur oxides, aromatics and formic acid present health concerns and potential maintenance issues. These should be considered when assessing the fuel's life-cycle environmental impact. The increase in emissions of those species correlates directly with fuel sulphur content (0.5% for neat TPO fraction), polyaromatic hydrocarbons fraction (0.49%) and acidity. Further optimisation of TPÓs composition in the reactor and via improved fuel post-processing can address these issues.

1. Introduction

Despite various attempts to introduce alternative powertrains for vehicle propulsion, internal combustion engines still offer a superior, rounded combination of functional features. This is especially true for off-road and marine sectors where robustness, energy density, economy and access to refuelling are challenging constraints for battery-electric or fuel-cell applications [1,2]. Nevertheless, these sectors are expected to comply with strict greenhouse gas (GHG) and pollutant emission limits reducing their environmental impact [3]. The above constraints are a stimulus to scale-up renewable alternative fuels that can be mixed into current fossil-fuel supply chains. So far, there are only two fossil diesel fuel (DF) substitutes that have reached commercial feasibility for heavy-duty transport and other heavy machinery powered by diesel engines [4]. The first of these, fatty acid methyl esters (FAME), can be produced from a variety of feedstock by a well-established and relatively simple transesterification process [5]. FAME may be used as stand-alone fuel but the current EN 590 fuel standard limits its automotive applications to 7% diesel admixture. Aside from some material compatibility issues and problems with oxidative stability, FAMEs typically reduce particulate emissions, especially at high engine loads, but tend to emit

* Corresponding author.
E-mail address: maciej.mikulski@uwasa.fi (M. Mikulski).

https://doi.org/10.1016/j.fuel.2022.123869
Received 18 January 2022; Received in revised form 9 March 2022; Accepted 11 March 2022
Available online 16 March 2022

Nomenclature

AHC	Aromatic hydrocarbon
BMEP	Brake mean effective pressure
BSFC	Brake specific fuel consumption
CA50	CAD value of 50% mass burned
CAD	Crank angle degree
CH_4	Methane
CI	Cetane index
CO	Carbon monoxide
CO_2	Carbon dioxide
CR	Common rail
DF	Diesel fuel
DI	Direct injection
DTPO	Tyre pyrolysis oil distillates
EGR	Exhaust gas recirculation
ELTEPA	End of life tyresUS Environmental Protection Agency
FAME	Fatty acid methyl esters
FTIR	Fourier-transform infrared
GC/MS	Gas chromatography/mass spectrometry
GHG	Greenhouse gas
GWP	Global warming potential
HCOOH	Formic acid
HRR	Heat release rate
HVO	Hydrotreated vegetable oil
IMEP	Indicated mean effective pressure
LCA	Life cycle analysis
MAP	Manifold absolute pressure
MFB	Mass fraction burnt
N_2O	Nitrous oxide
NO_X	Oxides of nitrogen ($NO + NO_2$)
OP	Operating point
PAH	Polycyclic aromatic hydrocarbons
PM	Particulate matter
SIM	Selective ion monitoring
SO_2	Sulphur dioxide
SoI	Start of injection
SoI_m	Start of injection (main injection)
SoI_p	Start of injection (pilot injection)
TDC	Top dead centre
TPO	Tyre pyrolysis oil
UHC	Unburnt hydrocarbons
λ	Excess air ratio (lambda)

more nitrogen oxides (NO_X), due to their oxygenated nature [6]. The second option, hydrotreated or hydrogenated vegetable oil (HVO), is an alternative biofuel of high quality and able to mix with DF in any proportions. Production of HVO is even more inclusive in terms of feedstock quality than transesterification [7]. HVÓs high volatility and good auto-ignition properties, together with its paraffinic chemical structure, support good combustion controllability and lower emissions, even when compared to conventional DF [8,9]. Even more recently, Hunicz et al. in a series of works [10,35] demonstrated that HVO is an enabler for achieving efficient Partially Premixed Compression Ignition (PCCI). By optimizing split injection strategies with boost and ultra-high EGR rates the authors noted indicated efficiency 1.5 percentage points above the optimised DF baseline, with engine-out NO_X and CO emissions near Euro VI limits.

Despite encouragement for renewable fuels, which have an annual growth rate of 4%, biofuels alone will not be able to cover the growing global demand for fuels [11]. Thus it is necessary to widen the choice of raw materials that can serve as renewable fuel feedstock. Pyrolysis is another process that yields liquid renewable fuels of a quality suitable for existing diesel engine technology. The important advantage of pyrolysis is that it supports the safe disposal of a wide range of synthetic feedstock, like rubber, plastic, etc. End-of-life tyres (ELT) in particular offer the twin benefits of high availability and low cost, plus the opportunity for clean, circular economy-based re-use scenarios [12]. Life cycle analysis (LCA) studies commonly indicate pyrolysis as the most environmentally friendly option for ELT utilisation [13,14]. Ultimately, tyre pyrolysis oil (TPO), the liquid fraction obtained from ELT pyrolysis, is considered a more favourable alternative to all first-generation biofuels in terms of carbon footprint [15]. Finally, co-pyrolysis of tyres with other bio and synthetic materials supports better process efficiency while improving TPO yield and its quality [16].

Recently, Mikulski et al. [15] presented an exhaustive review of TPO combustion engine applications. The state of the art presented in that work is distilled below to give context to the present work. Looking at commercial TPO production, there are currently at least five different reactor designs used to process TPO, including fluidised bed [17]; fixed bed [18]; moving bed [19]; spouted bed [20]; and relatively recent rotary kiln designs [21]. Dependent upon reactor type, the processes usually involve different catalysts and inert gases. Their synergistic effect maximizes the yield of the liquid fraction, with the best performance reaching 80% [22], coupled with a high calorific value of up to 44 MJ/kg [23] The key variables for optimum results are the reactor type and catalyst used. The best performance is generally derived from fast pyrolysis, with temperatures between 450 and 650 °C [15]. Increasing the process temperature beyond this point shifts the yield towards the gaseous fraction. Higher process temperature also leads to an unfavourable increase in TPO viscosity and supports sulphur and aromatic penetration from solid substrates to the liquid products. Typical viscosity of crude TPO ranges between 839 g/dm3 to 904 g/dm3) [24], and sulphur concentration is from 0.3 to 1%[25].

Cutting-edge production technology endows crude TPO with sufficient quality to be used directly as bunkering fuel [26]. Alternatively, it can be further processed to provide quality close to the EN 590 or ASTM D975 on-road diesel fuel standards. Application of ionic solutions/liquid–liquid extraction may be perceived as an interesting, low-cost alternative to refinery hydro-desulphurisation [27,28]. Further post-processing measures include distillation and fractional blending. TPO distillates (DTPO) generally offer low viscosity and good cold properties, but their flash point is too low to meet automotive diesel standards. However, viscosity and flash point do not scale linearly with distillation temperature, paving a feasible route for DTPO application as a viscosity improver for FAME or straight vegetable oils [29,30]. Note that fractions that would be driven by distillation curve analysis, with contemporary engine fuel properties in mind, have not been considered so far.

Auto-ignition properties of TPO are different from DF́s. It is commonly agreed that TPO's lower cetane index (CI) delays combustion [31,32], resulting in deterioration of engine efficiency, as reported by Sharma et al. [33], Martinez et al. [34] and Murugan et al. [35]. However, it has been proven that admixtures of crude TPO to conventional diesel, in amounts not exceeding 10%, may be used as drop-in fuels without any negative effects during combustion or manifesting in reduced thermal efficiency [24,36]. Specific fractions of DTPO may be used even in greater concentrations without any significant undesirable effects on combustion [35].

TPÓs impact on emissions is complex and involves both (i) physical properties that affect atomisation and mixture formation, and (ii) chemical propensity to create specific species. Most of the available reports indicate that TPO admixture increases carbon monoxide (CO) and unburnt hydrocarbons (UHC) emissions, which can be attributed to higher viscosity. It suppresses fuel atomisation, limiting oxygen

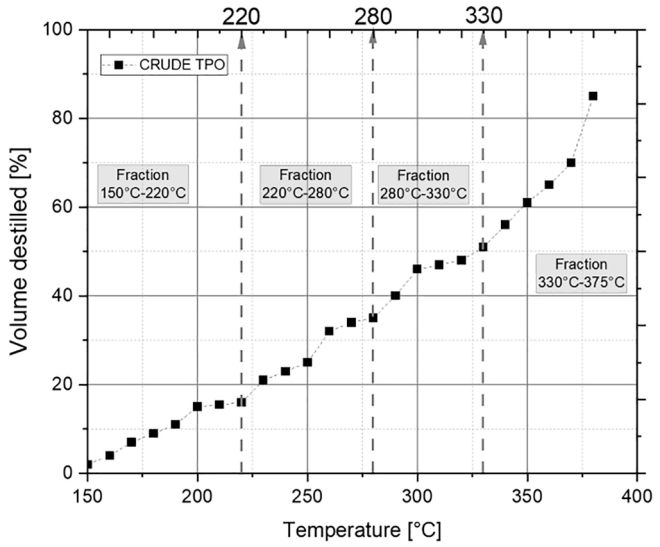

Fig. 1. Distillation curve of crude TPO, with division into fractions. The fourth fraction (330–375 °C) was used to compose samples for engine tests.

Table 1
Fuel analytics methods applied in this study for diesel, TPO and their blends.

Property	Method - standard	Method - description	Uncertainty level	Unit
Density @ 15 °C	EN ISO 3675	Areometer	0.01	kg/m^3
Viscosity @ 40 °C	EN ISO 3104	Ubbelohde viscometer	0.008	mm^2/s
Flash point	EN ISO 3679	Closed-cup Pensky-Martens	0.5	°C
Sulphur content	EN ISO 20,884	X-ray reflection	0.4	ppm
Water content	EN ISO 12,937	Coulometric titration	0.1	mg/kg
Copper corrosion @ 3hr/50 °C	EN ISO 2160	Copper strip test	–	Class[1)]
Higher heating value (HHV)	D 4809–95	Bomb calorimeter	0.2	MJ/kg
Cetane index (CI)	EN ISO 4264	Derived from distillation curve and density	0.1	–
Hydrocarbon analysis	na	Gas chromatography and mass spectrometry (GC–MS)	na	mg/kg

[1)] Classes ranging from 1A (slight tarnish; a - almost the same as a freshly polished strip) to 4C (corrosion; c - glossy or jet black)

entrainment to the developing fuel spray [37]. On the other hand, TPÓs low cetane index (CI) supports the creation of lean premixed fractions which are not oxidised completely [38]. Notably, the increment of the emissions is highly correlated with the amount of the TPO (or its fractions) in the final fuel blend. NO_X emissions are also commonly reported as increased by TPO. This may be partially explained by higher amounts of molecular nitrogen inside the TPO particles, compared to conventional fuels [34]. Additionally, delayed auto-ignition associated with TPO's lower CI (compared to DF) shifts combustion towards a more premixed mode, giving increased heat release rates and peak temperatures, thus promoting NO_X formation [32]. However, several studies report a reduction of NO_X emissions, indicating lower combustion temperature as the prime factor [37]. This ambiguity of the results is possible because the effect of combustion timing on NO_X formation is not linear. The optimal delay of combustion shifts the process towards a low-temperature regime, significantly reducing NO_X emissions [39].

TPO and DTPO fuel mixtureś high aromatic content make them prone to increased particulate matter (PM) formation [40]. Significant amounts of solid contaminants in TPO, formed during pyrolysis, are also believed to promote PM formation [41]. The particular disadvantage is that pyrolysis-derived fuels may form smaller - and thus more hazardous - particulates than those derived from the combustion of diesel fuel [42,43].

Optimising fuel injection control, including pressure and timing, as well as proper thermal management (airpath control), may eliminate some of these negative effects of the aforementioned undesirable TPO/DTPO properties [32], but only the physical ones. Optimisation of injection is limited by the possibility of spray wall-wetting. However, preheating the fuel [44], or increasing the intake temperature can be advantageous.

The above brief description of TPO properties, upgrading perspectives and typical problems related to engine application, summarises the latest thinking and studies. However, so far there has not been a single study that provides a comprehensive evaluation of modern, industry-standard pyrolysis-derived fuel in a contemporary engine. Studies focused on crude TPÓs production usually correlated the fuéls detailed characteristics with pyrolysis process conditions and feedstock quality [45]. They did not follow up with tailored upgrading to produce a chemical make-up designed for optimum engine operation, not to mention subjecting it to end-validation on the engine test stand. On the other hand, engine experimentalists typically assume TPO as generic fuel without considering quality differences related to production or upgrading [26]. Most engine studies have not even considered a detailed chemical make-up of the tested fuel to explain the differences in performance and emissions [46]. Most of the knowledge summarised in the introduction regarding combustion and emissions comes from legacy (pre-Euro standard) engine platforms. Tests results involving combustion principles pertaining to contemporary engines are not available. Finally, the issue of unregulated emissions, especially polyaromatic hydrocarbon emissions and their trade-off with PM formation, is not studied at all for TPO-derived fuels, leaving a significant knowledge gap.

The present work aims to address these deficiencies and gaps. The paper, for the first time, provides a state-of-the-art combustion analysis of tailored TPO fractions obtained from a fully identifiable source. To this end, the production process of crude TPO is scrutinised and supported by detailed analytics of its targeted distillates. The final blends are selected for engine tests, taking into account the overall availability/compatibility of TPO fractions with diesel. The modern, single-cylinder research engine used for testing enables evaluation of sophisticated, multi-pulse injection strategies under fully controllable thermal conditions across a range of air/exhaust gas recirculation (EGR)/fuel ratios. The issue of unregulated emissions is handled by Fourier-transform infrared (FTIR) analysis of exhaust gases, including identification of 23 species.

2. Materials and methods

2.1. Test fuels and fuel analysis methods

The TPO used for testing was manufactured using an industrial-scale (8-tonne feed capacity), rotary kiln reactor operating in the intermittent feed mode. Compressed and packaged light-duty vehicle tyres were fed directly to the reactor without any pre-processing. The TPO was discharged from the reactor as vapour and, after condensation, subjected to two-step filtration, including a Buchner funnel with 13 mm-mesh at the fine-filter side. We have discussed the pyrolysis process comprehensively, including its relevant control parameters, in another work by Duda et al. [47].

To reduce viscosity and polycyclic aromatic hydrocarbons (PAH) content, the crude TPO was further distilled to four fractions in temperature ranges of 150–220 °C, 220–280 °C, 280–330 °C and 330–375 °C. Fig. 1 depicts the distillation curve for crude TPO for

Table 2
Research engine specifications.

Type	AVL 5402
Configuration	four-stroke, single-cylinder
Bore	85 mm
Stroke	90 mm
Displacement	510.5 cm^3
Compression ratio	17:1
No. of valves	4
Swirl ratio	1.7:1
Combustion type	direct injection
Max. fuel injection pressure	180 MPa
Injection system	common rail, Bosch CP4.1
Boost system	electrically driven Eaton M45 compressor
EGR system	high-pressure, cooled
Engine management	AVL-RPEMS, ETK7-Bosch
Intake valve opening	712 CAD[1)]
Intake valve closing	226 CAD[1)]
Exhaust valve opening	488 CAD[1)]
Exhaust valve closing	18 CAD[1)]
Max. engine load (IMEP[2)])	2.4 MPa

[1)] Crank angle degree.
[2)] Indicated mean effective pressure.

reference. The fractions were photographed for visual comparison. One can refer to Appendix 1 for this material.

The distillates obtained were then subjected to solid residue elimination and desiccation, using percolation and filtration with silica gel and anhydrous sodium sulphate beds, respectively. The TPO samples were subjected to basic physical and chemical analysis to verify their suitability as fuel or fuel additives. The analysis methods followed the respective standards for the usability of diesel and diesel alternatives. Table 1 lists these methods, including device uncertainty level.

The same analytical methods were applied for all fuel samples subjected to engine tests. The heaviest TPO fraction (330–375 °C), referred to as F4, was used to create blends with EN 590/ASTM D975-compliant automotive diesel. The binary mixtures, with TPO content of 20% and 40%, denoted as TPO20 and TPO40 respectively, were subjected to engine tests. The selection of final engine blends was guided by an in-depth consideration of blending strategies [47]. At this point, it is sufficient to say that the primary objectives for the blends were acceptable sulphur content, flash point and viscosity, while balancing the anticipated demand for individual TPO fractions to suit the needs of different fuel quality requirements. To this end, the present study focused on fuels for off-road machinery, as outlined in the premise stated in the introduction. Thus, the ASTM D975 standard No. 4-D was used as guidance for engine fuel quality targets. ASTM D975 is the US standard for diesel fuels: grade No. 4-D is for middle distillate fuels and blends, suitable for use in low- and medium-speed engines in applications necessitating sustained loads at a substantially constant speed.

2.2. Engine research

2.2.1. Experimental set-up

Experimental works were performed at the Lublin University of Technology. A four-stroke, single-cylinder AVL research engine, type 5402 common-rail (CR) direct injection (DI), served as the research object. The engine had a displacement of 510 cm^3 and a compression ratio of 17:1. The combustion system was based on a four-valve head with tangential and helical ports to control swirl, and a toroidal, in-piston combustion chamber. Fuel was injected via a seven-hole solenoid injector with an included spray angle of 145°. Injection control was via a fully open Bosch engine control unit managed by ETAS INCA software. The supplied fuel was thermally conditioned by the AVL 753C temperature conditioner. Fuel consumption was measured by an AVL 733S dynamic fuel meter. Table 2 presents the main specifications of the tested engine.

The engine was equipped with a fully controllable air-path, which included an electrically driven Roots compressor (Eaton M45) and a high-pressure, cooled EGR loop. The exhaust runner had a plenum chamber and backpressure valve to mitigate turbocharger operation and force exhaust gas flow through an EGR valve. There was independent

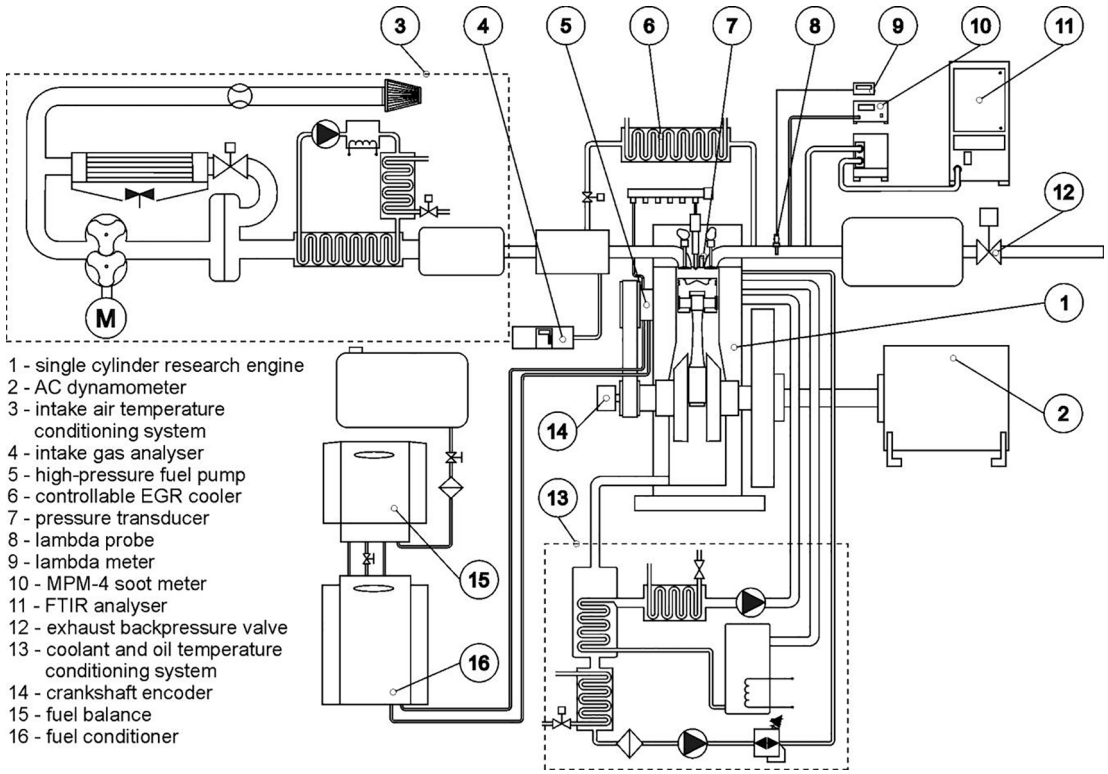

Fig. 2. Diagram of the SCRE engine test bench in the Lublin University of Technology. Only major subsystems and measurement devices indicated.

Table 3
Engine test bench measurement equipment and accuracy.

Measurand	Transducer		Meas. range	Accuracy
In-cylinder pressure	AVL GU22C		0–25 MPa	0.25–1.0%[1)]
Fuel consumption	AVL Fuel Mass Flow Meter 733S		0–125 kg/h	0.12%
Excess air ratio (λ)	Bosch LSU 4.2 / ETAS LA4		0.7–2.8	1.5%
Air mass flow rate	E + E Elektronik EE741		2.6–1000 kg/h	3%
Intake/exhaust press.	WIKA A-10		0–4 bar	0.5%
Temperatures (ambient, intake air, EGR, cooling, oil, fuel)	Pt100 Czaki TP-361		−40–400 °C	0.2%
Exhaust temperature	Thermocouple K Czaki TP-204		0–1200 °C	0.8%
Exhaust composition (gaseous compounds)	AVL Sesam FTIR	CO: UHC: NO_X:	1–10000 ppm 1–1000 ppm[2)] 1–4000 ppm	0.36% 0.1–0.49%[3)] 0.31%
PM concentration	Maha MPM4		0–700 mg/m^3	0.1 mg/m^3
Intake composition	Hermann-Pierburg HGA 400	CO_2: O_2:	0–20% 0–22%	0.1% 0.01%

[1)] Depending on temperature.
[2)] Given measurement span relates to the concentration of a single identified hydrocarbon.
[3)] Depending on the type of hydrocarbon species.

Table 4
Tested operating points OP1-OP5 corresponding to the D1-Type ISO 8178 test cycle for constant-speed gen-set applications. The secondary data in brackets refer to the EGR calibration when different from non-EGR calibration.

Operating point	OP1	OP2	OP3	OP4	OP5
Load [%]	100	75	50	25	10
BMEP[1)] [MPa]	1.3	0.975	0.65	0.325	0.13
MAP [kPa]	180	156	140	125	100
EGR [%]	0	0	0 (10)	0 (20)	0 (40)
λ [-]	1.54	1.68	1.95 (1.74)	2.74 (2.15)	5.28 (3.11)
Intake Temperature	36.2	36	35.6 (41)	35.5 (44.3)	35.5 (50.4)
SOI_p[2)] [CAD]	340	340	340	342	344 (342)
SOI_m[3)] [CAD]	356	356	356	356	356 (354)
Fuel pressure [MPa]	80	80	70	60	50
Pilot fuel quantity [mg]	1.7	1.7	1.7	1.6	1.5
Pilot fuel fraction [%]	4	5	7	10	20
Emission factor	0.05	0.25	0.3	0.3	0.1

[1)] Brake mean effective pressure.
[2)] Start of pilot fuel injection.
[3)] Start of main fuel injection.

temperature control for both the air after the compressor and the EGR circuit.

The test stand was equipped with an in-house thermal conditioning system to maintain coolant and lubricant at constant temperatures, to within +/- 0.5 °C accuracy. Pressure and temperature transducers mounted in several locations of the air-path provided additional parameter monitoring. Fig. 2 depicts the test stand set-up: Table 3 lists the measuring devices and their accuracies.

To replicate operation under normal service conditions, the engine was coupled to an asynchronous motor dynamometer from AVL. The dynamometer control system governed rotational speed and engine torque requirement. For the combustion analysis, a piezoelectric pressure transducer (AVL GU22C) was installed in the engine head. Recording of the high-speed pressure signal was triggered using an optical encoder, with a constant angular resolution of 0.1 CAD.

Exhaust gas samples were received by an AVL FTIR multi-component analytical system, measuring concentrations of 23 regulated and unregulated exhaust gas components. A Maha MPM-4 analyser measured the particulate concentration. A Bosch LSU 4.2 lambda probe and ETAS LA4 lambda meter recorded the excess air ratio (λ), with pressure compensation [48]. The carbon dioxide (CO_2) ratio between the intake and the exhaust gas was used to calculate the EGR rate. A Hermann-Pierburg HGA 400 gas analyser was used to measure CO_2 on the intake side.

2.2.2. Scope and conditions of the tests

The fuels were tested according to the ISO 8178 type D2 test for stationary engines. The test comprised five operating points (OP), representing a load sweep performed at rated engine speed. In the research engine, this was set to 1500 rpm, typical for use with a dual-wound 50 Hz electric generator. The measurements were performed for two engine calibrations: one for an engine without external EGR, one for an engine with variable EGR. Both calibrations were created for the reference DF and aimed at minimum overall emissions with constrained indicated thermal efficiency above 45%. Accordingly, a split-injection strategy was used, with an early pilot injection followed by main injection, close to the top dead centre (TDC), to directly control the start of combustion. This approach is typical of that used in the latest diesel engines. Table 4 lists the engine calibration details for all operating points of the ISO 8178 test cycle.

The calibrated points had individual fuel-rail pressure, start of injection (SOI) and pilot fuel fraction set-points. Manifold absolute pressure (MAP) was generally increased with load to provide sufficient oxygen at elevated fuel values. Refer to air–fuel ratios (λ) in Table 4 for details on the in-cylinder mixture conditions. Note, that during the variable-EGR calibration, the global best emission results at elevated loads were obtained with the EGR valve fully closed. Thus, EGR was applied only for three operating points (OP3-OP5); test conditions at OP1 and OP2 are the same for both the non-EGR and EGR calibration.

The intake air temperature was maintained at a constant level of 36 +/-0.5 °C regardless of the brake mean effective pressure (BMEP). Temperatures of the engine coolant and lubrication oil were set at 85 °C, the same as the temperature of recirculated exhaust gas entering the intake manifold. Note that the temperature of air aspirated by the engine resulted from the enthalpy balance between boost air and EGR, which was left uncontrolled. The temperature of fuel going to the high-pressure pump was set at 30 °C.

The first tests were with the DF baseline, followed by the blends TPO20 and TPO40, which were tested according to the same procedure. In order to ensure the assumed proportions of the tested fuels, during each fuel change, the entire fuel system was thoroughly drained and then flushed several times with the new fuel sample.

For each tested fuel, the test sequence was repeated three times, where engine loads were changed in a different order. At each OP, after stabilisation of all parameters, the in-cylinder pressure was recorded for 100 cycles and slow-changing data were recorded during the 30-second measurement period. The presented data are the mean values of the three engine runs at each OP.

2.2.3. Data analysis routines

Combustion analysis was based on in-cylinder pressure measurement. The raw measurement signal was pegged, filtered and cycle-averaged. The pegging (absolute pressure referencing for the relative in-cylinder pressure sensor) was performed using the intake port pressure signal values at cylinder bottom dead centre/intake valve opening coincidences. The start of ignition, for subsequent combustion phases (refer later to Fig. 7), was determined by the second pressure derivative method. The method detects local peaks in pressure rise acceleration and is proven more robust for complex multi-injection strategies than

Table 5
Physical and chemical properties of the fuels used in the research.

Parameter	Unit	DF	TPO crude	TPO F4	TPO20	TPO40	ASTM D975 (reference)	
							No. 2-D	No. 4-D
Density @ 15 °C	kg/m^3	826	939	948	844	867	n/a	n/a
Viscosity @ 40 °C	mm^2/s	2.3	3.7	15.3	3.0	3.9	1.9–4.1	5.5–24
Flash point	°C	61	25	90	61	61	>52	>55
Sulphur content	mg/kg	6,1	7400	5000	1154	2265	<15	n/a
Water content	mg/kg	11	1450	410	86	141	<500	< 500
Copper corrosion	class	1A	1A	1A	1A	1A	<3A	<3A
HHV	MJ/kg	44.8	44.1	44.7	44.7	44.8	n/a	n/a
CI	–	40.1	33.8	32.6	38.2	36.1	>40	>33

commonly used heat release-based routines [49]. Further post-processing of the in-cylinder pressure was performed using AVL Boost software, which incorporated first-law analysis to provide the heat release rate (HRR). Note that AVL Boost improves the HRR calculation accuracy by resolving a detailed 1-dimensional gas exchange model to estimate internal residuals. The HRR values in all the figures discussed here are apparent (gross), corrected for the heat transfer through cylinder boundaries. The cylinder wall temperatures were estimated, case dependently using AVL Boost, and a well-established Hohenberg correlation for heat transfer coefficient was used in the heat-loss model [50]. The cumulative HRR was further used to calculate mass fraction burnt (MFB), which yielded combustion timing indicators, like crank angle location of 50% mass burned (CA50).

The directly measured molar concentrations of exhaust gas components were converted to brake-specific emissions, with consideration of the brake specific fuel consumption (BSFC), excess air ratio and atomic fuels compositions. Note that FTIR emission measurements were done directly using "wet" effluent gases. The PM emission was directly measured on the mass per volume basis (Table 3) and accordingly converted to brake-specific values. This brake-specific, "wet" representation of the results is in line with the EPA Tier 4 emission standard used as a reference in this research.

Device uncertainty listed in Table 3, was assumed as the maximum measurement error for directly measured values. The measurement error for indirectly calculated values, like brake-specific emissions, was established from the derivatives of directly measured inputs and their errors, according to the partial derivative method by Kline and McClintock [51]. For details on the application of this method towards uncertainty analysis in contemporary engine research, the reader is referred to another work by the authors [52]. Aside from measurement error, in engine tests, the disturbances cause significant statistical error related to the unrepeatability of initial conditions. This was minimised by conditioning the intake and fueling paths, as described in section 2.2.1. Still, to assess this phenomenon all measurements at individual operating points were repeated in different sequences, as outlined in section 2.2.2. Finally, a measurement error or standard deviation (whichever was higher) was used as an uncertainty indicator for the emission results and selected combustion indicators.

3. Results and discussion

The results discussion adopts a cause-to-effect structure. First, in section 3.1, the results of the fuel characterisation are analysed, giving insight into the fuels' properties influencing combustion and emission. Then, in section 3.2, selected results of the combustion analysis are discussed to underline in which regions of the map the tested TPO samples behave differently from the diesel reference. This further allows understanding the differences in emission and performance characteristics amongst the tested fuels. So, in sections 3.3 and 3.4 we decouple the effects of fuel chemistry on emission formation from the effects related to combustion. Section 3.3's emphasis is on conformity with relevant emissions standards, while section 3.4 focuses on unregulated emissions and the greenhouse gas effect of the tested fuels.

3.1. Fuel characterisation

Table 5 presents the results of the basic physical and chemical analytics of the five fuels in this research. Three of them, the DF and the blends TPO20 and TPO40, were used for the engine tests. Note that several requirements for diesel engine fuels in different transport domains were considered when targeting the TPO blends. Refer to Mikulski et al. [15] for a comprehensive review of fuel standards applicable to TPO-derived fuel. Note also that the automotive and marine/stationary engine fuel regulations are considered the two boundary regimes for TPO applicability (least and most inclusive, respectively). For brevity, Table 5 includes only the US ASTM D975 on-road (No. D-2) and stationary (No. D-4) engine fuel standards to provide context to the discussion.

The challenge for the tested blends to satisfy ASTM D975 requirements is apparent in Table 5. Critical drawbacks of crude TPO are excessive sulphur content, high viscosity and low flash point, rendering distillation and desulphurisation necessary.

While density scales almost linearly with the content of TPO F4, the blending strategy benefits from the non-linear effect of TPO additivation on viscosity. TPO40's viscosity is only 1.7 times higher than DF's, while the eqivalent ratio for its substrate, TPO F4, is 6.7. The reference DF has a viscosity improver, thus thinning the blends [53]. Elevated viscosity and density of the TPO20/40 samples can impinge on fuel atomisation in the spray, resulting in increased UHC, CO and PM emissions and related deposit formation. Nevertheless, these fuel parameters are in line with statutory limits for both automotive and off-road applications, so the effect is expected to be minor.

The flash point indicates the temperature at which the fuel forms ignitable vapours in ambient conditions. Safety concerns dictate that this must be no<52/55 °C in the two ASTM D975 applications. The flash point will be determined by the most volatile fraction in the mixture, so both TPO20 and TPO40 blends inherit the value of more volatile DF (61 °C) in the test, despite TPO F4's much higher flash point of 90 °C.

Although the flash point gives some indication of mixture volatility, and thus influences physical ignition delay, it does not directly determine ignitibility in engine-relevant conditions. For this purpose, the CI has been evaluated for all mixtures, using their specific density and mid-boiling point temperature dependencies (Table 1). This allows comparison of the fuel's chemical ignition delay. The CI of TPO F4 is roughly 20% lower than DF's, and with a value of 32.6, is slightly below the relevant ASTM limit for off-road applications. This means its use as drop-in fuel in diesel engines would require preheating. This CI disadvantage diminishes in the blends but TPO20 and TPO40 still are expected to experience prolonged ignition delays, especially in areas of the map where EGR is used [10].

TPO fuels commonly are reported to contain carboxylic acids [54]. Accordingly, this research measured their corrosion on a copper strip to assess potential impact on fuel system components. Interestingly, both the crude TPO and its fractions achieved the same highest category 1A (no noticeable effects - the same as a freshly polished strip.) Still, the elevated acidity of the fuel can manifest in the formation of formic acid in the exhaust. After sulphur, this is a second relevant factor responsible

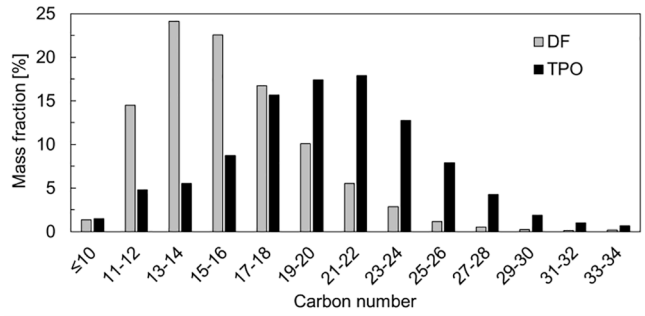

Fig. 3. Hydrocarbon distribution of TPO F4 and DF from the full-scan GC–MS.

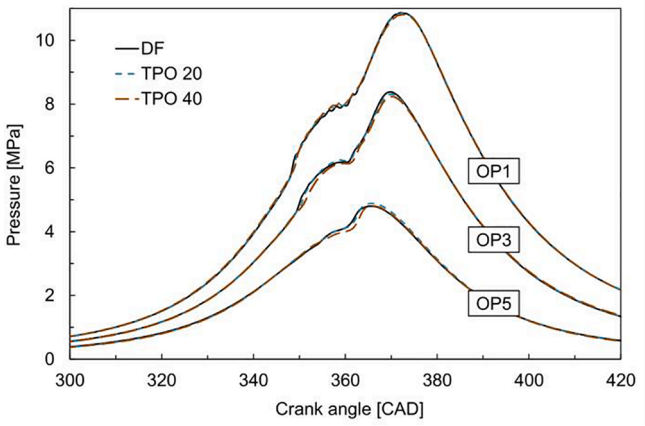

Fig. 4. In-cylinder pressures for the representative operating points of the none-EGR calibration; 10% load (OP5); 50% load (OP3) and 100% load (OP4).

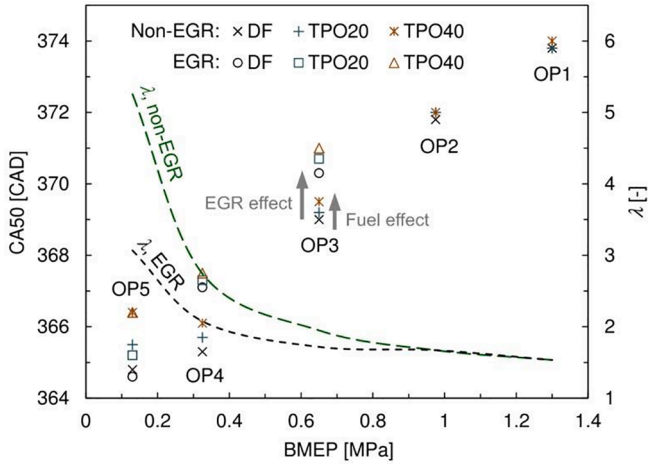

Fig. 5. The combustion phasing (CA50) and the air–fuel ratio (λ) for the non-EGR and variable EGR calibrations.

for poisoning of aftertreatment systems [55]. This is separately assessed during the detailed emission tests.

Sulphur content is by far the most limiting factor for TPO. The ASTM D975 4-D standard itself does not include a sulphur limit but there are several incentives to cut sulphur in a wider context. The obtained values for TPO20 and TPO40 can meet the requirements of the International Maritime Organization global sulphur cap [56]. TPO20 can comply with the 0.2% sulphur limit (2000 ppm) for fuel used during certification testing for EPA Tier 1–3 emission legislation, still applicable in many countries for off-road engine certification [57]. Note that Tier 4, used as a reference for normative emissions discussion in section 3.3, already assumes using ultra-low sulphur diesel (7–15 ppm sulphur content). It is hard to expect that any TPO post-processing measures, aside from refinery-grade hydro-desulphurisation, can meet this target, so high sulphur content remains a challenge when considering decentralised TPO production in the future. The influence of TPO-bound sulphur on regulated and unregulated emissions is further discussed in sections 3.3 and 3.4.

Turning to the issue of water content, simple and inexpensive anhydrous sodium sulphate bed moisture removal allows TPO to comply with fuel quality standards. As shown in Table 5, this process, together with distillation, decreased the water content by 70% (compare the values of TPO-crude and TPO F4). Consequently, the TPO20 and TPO40 samples meet the strict automotive fuel standards with a decent margin. Furthermore, the TPO F4 used here has a higher heating value (HHV) of 44.7 MJ/kg, very close indeed to DFs 44.8 MJ/kg, bearing in mind the measurement uncertainty level of +/-0.2 MJ/kg (Table 1). This beneficial characteristic was confirmed in the engine tests, where recorded fuel consumptions at each operating point did not change noticeably between DF, TPO20 and TPO40. At this point, it is worth noting that DF used in this research did not contain any biocomponents. None of the engine test fuels (DF, TPO20, TPO40) contained any oxygen that could influence the emission analysis results, further discussed in sections 3.3 and 3.4.

Fig. 3 concludes the fuel analytics, highlighting the fundamental differences in hydrocarbon make-up between DF and the TPO F4 used to compose TPO20 and TPO40. DF is composed mostly of lower hydrocarbons (C_{11}-C_{18} particularly), while compounds with carbon numbers above 21 account for as little as 10.6% of the total mixture mass. TPO F4, on the other hand, is mainly hydrocarbon chains between C_{17} and C_{24} with an overall share of C_{21} and higher topping 46.4%.

At this point, it should be noted that detailed hydrocarbon analysis for pyrolytic oils is generally challenging due to the particularly complex chemical structure of components with similar boiling points. Specifically, retention times in the rectification column are similar in TPO, so mass spectrometer intensity peaks interfere with each other. The full-scan GC–MS spectrograms in Appendix 2 show more detail of this. This issue, amongst others, prevented the verification of the on carboxylic acid content in TPO, raised earlier in the discussion. Note that this hypothesis will be still verified based on emission results in section 3.4.

TPÓs hydrocarbon distribution, coupled with the CI results, yield interesting hypotheses on its qualitative composition. In general, normal paraffins and olefins that typically cover a wide range of fuel's hydrocarbon distribution, yield increasing CI with the increasing share of higher carbon molecules. The fact that this trend is not seen between C < 18-dominated DF and TPO F4 dominated by higher carbon numbers implies a large share of aromatics in the TPO fraction, with a particular issue concerning PAH. Bearing this in mind, a dedicated selective ion monitoring (SIM) GC–MS test was performed for the presence of PAH in both DF and TPO F4. The cumulative content of PAH in TPO was measured at 0.49% on a mass basis, which is six times more than in DF. Acenaphthene, pyrene, benz(a)anthracene and chrysene were the largest PAH contributors. These are heavily carcinogenic when transferred to the air as combustion products, so must be considered when contemplating TPÓs applications as a fuel admixture.

3.2. Combustion analysis

The in-cylinder pressures for the representative low-, mid- and high-load operating points are provided in Fig. 4. Consequently, Fig. 5 outlines the trends in combustion phasing (CA50) for all OPs including separate calibrations for an engine without EGR, and one incorporating external, high-pressure EGR. Looking at the DF combustion indicators in Fig. 5, one can note that CA50 shifts towards the expansion stroke with increasing load. Retardation of the onset of combustion between OP3

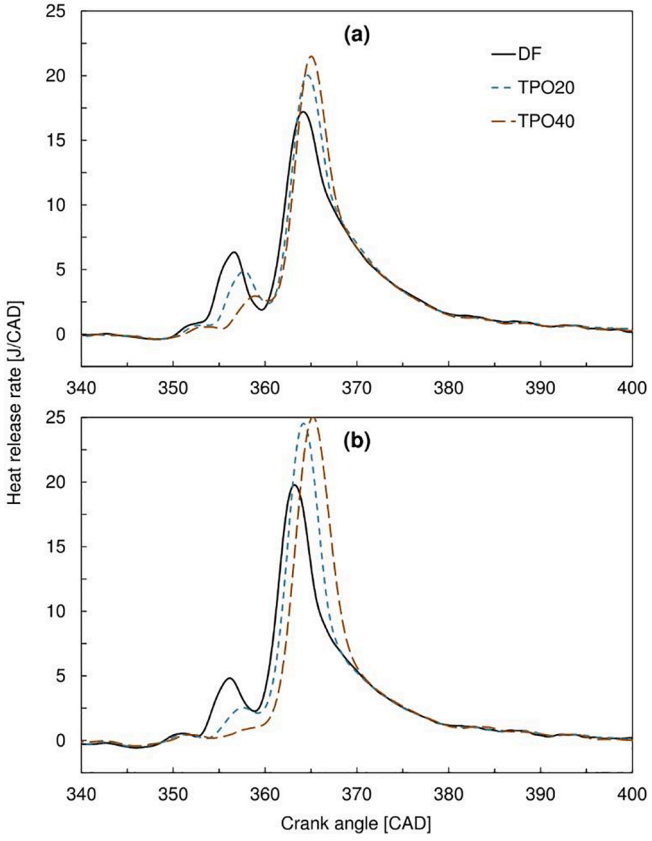

Fig. 6. Heat release rates for the low-load case (OP5) with non-EGR (a) and EGR (b) calibrations. Note that for EGR conditions injection timings were advanced by 2 CAD.

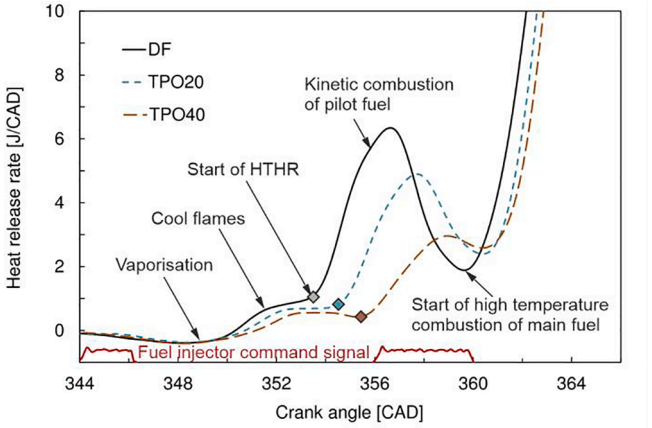

Fig. 7. Zoom-in on Fig. 4s pilot fuel combustion phases: heat release rates at low load (OP5) with non-EGR calibration. Respective grey, blue and orange diamonds indicate the start of combustion of the high-temperature heat release rate of the pilot fuel. (For interpretation of the references to colour in this figure legend, the reader is referred to the web version of this article.)

and OP1, with fairly constant injection timing and intake temperature (refer to Table 4), is the result of reduced λ, as the MAP increment does not scale proportionally to the total fuel value. Nevertheless, the start of main fuel combustion appears near TDC, evident from the detailed heat release rates in Fig. 6 and Fig. 7. This strategy aims to keep NO_X within the emission limits, while maintaining high thermal efficiency.

Reverting to fuel-to-fuel differences, the key point to emerge from Fig. 4 and Fig. 5 is that, in the explored combustion regime, sensitivities

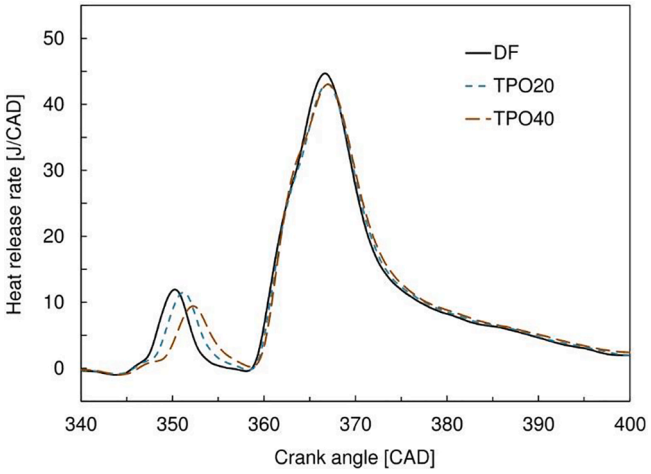

Fig. 8. Heat release rates at the mid-load case (OP3) with 10% EGR.

appear only at low engine loads. The trends in CA50, however, are not monotonic at first glance and the fuel effects appear to be an order of magnitude smaller than those associated with EGR or MAP-related λ change. CA50′s weak sensitivity to fuel is attributed to the second injection, initiated close to TDC. This acts as a direct combustion trigger for the main combustion event. Note that at OP5, the EGR effect is compensated by 2 CAD advance of injection timing (Table 4).

Fig. 6 gives phenomenological insight into the mechanisms of combustion at low loads. Despite apparent insensitivity in CA50, the combustion is phenomenologically affected by the tested fuel properties. For both low-load cases (Fig. 6a and Fig. 6b), after pilot fuel injection and its vaporisation (negative heat release due to evaporative cooling), the low-temperature combustion phase starts with a 5 CAD ignition delay. Since there is sufficient time for the fuel to premix, and both blends contain highly reactive DF components, differences between fuelś viscosity do not affect the start of cool flame reactions. For the non-EGR case (Fig. 6a), the relation of the cool flame reactions to pilot injection timing is presented in Fig. 7.

It is apparent from Fig. 7 that the volumetric, kinetic combustion follows the cool flames. This is highly sensitive to fuel properties. The CI, characterising the chemical auto-ignition properties of the individual test fuels, plays a key role in this sensitivity. The kinetic combustion of the pilot becomes proportionally delayed with the increase of TPO concentration, by approximately 1 CAD for each 20% of admixture. This corresponds to a CI reduction of 5%, as depicted in Table 5. The maximum HRR in this stage is correspondingly reduced for the TPO samples; TPO40́s maximum HRR is half that of the DF reference. This corresponds to less fuel undergoing combustion before the main fuel dose ignites at approximately 358 CAD - almost instantly after the injection cone reaches the burned zone from the pilot. Detailed analysis of DF́s cumulative heat release reveals that at this crank angle, around 10% of the total fuel mass (roughly 50% of the pilot injection) has undergone combustion, whereas for TPO40 the mass of fuel burned at this point was less than half that figure. This energy surplus is then released during the main combustion, giving correspondingly elevated peak HRR values and elongated combustion duration for TPO20 and TPO40, as apparent in Fig. 6a.

Reverting to Fig. 6b, depicting heat release rates for the EGR calibration, one can note that the fuel effects are qualitatively the same as for the non-EGR case discussed earlier. The addition of EGR further suppresses premixed combustion of the pilot fuel, and the lower CI of the TPO blends makes them more vulnerable to this phenomenon. Note, that for TPO40, the premixed combustion of the pilot is practically absent. Consequently, the main injection does not meet the burning region of the pilot, resulting in the main combustion phase being delayed by almost 3 CAD compared to the DF reference. This shift of the main heat

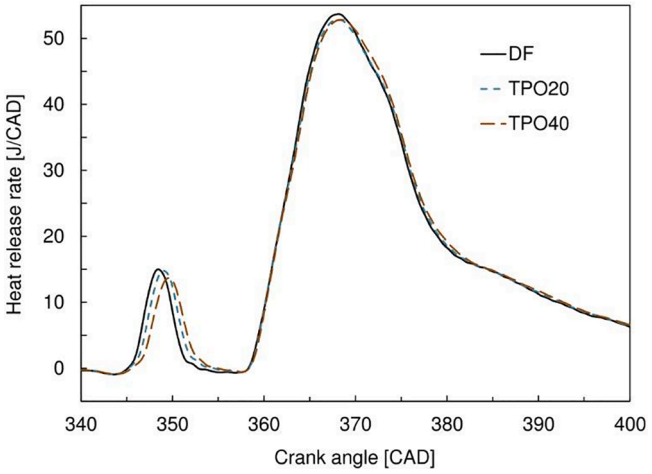

Fig. 9. Heat release rates at the high-load case (OP1).

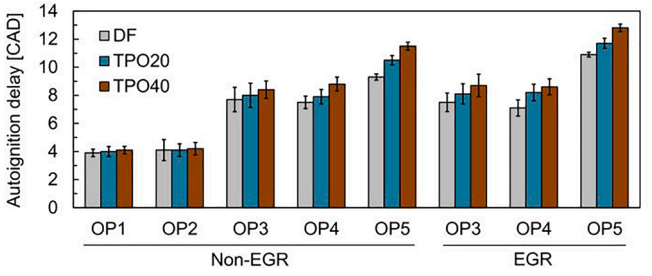

Fig. 10. Autoignition delay, defined with respect to the start o the high-temperature combustion phase of the pilot fuel (see Fig. 7). Results for both EGR and Non-EGR calibrations.

release towards the expansion phase ultimately slows down combustion. The increase in peak HRR caused by the pilot fuel surplus being transferred to the main combustion is thus mitigated, compared to the non-EGR case. The first effect explains the sensitivity in combustion phasing observed for TPO-based fuels at low-load and heavy EGR conditions (Fig. 5). The second phenomenon will have a substantial effect on emission formation. Generally, the diffusive main combustion phase carries the highest local combustion temperatures, and elevated peak HRR correlates to peak bulk temperature of the in-cylinder mixture. TPO tends to combust more through a diffusive spray flame at low loads, whereas DF exhibits more distinctive premixed combustion characteristics. The elevated combustion temperatures for TPO will translate into differences in NO_X and PM emissions which are driven by thermal mechanisms. We will discuss this further in the following sections.

According to Fig. 5, the higher the engine load, the less significant is the effect of fuel on combustion phasing. This can be reviewed in Fig. 8 and Fig. 9, depicting HRR for mid and high-load cases. For OP3 (50% load), the high-temperature combustion of pilot fuel is still delayed and HRR is cumulatively reduced in this phase by TPO admixture. This is akin to the low-load case of Fig. 6a, but quantitatively far less pronounced. The weaker sensitivity in the pilot phases means that the main, diffusion-controlled combustion phase runs nearly along the same line for all tested fuels. In the case of the highest load point (OP1), the differences in the fuelś main combustion characteristics disappear almost completely, although differences in their pilot combustion trends, clearly seen at lower loads, are still apparent at 100% load, depicted in Fig. 9.

The EGR effects discussed in the case of OP1 in Fig. 6b are qualitatively the same for all load points. However, fuel-to-fuel differences diminish with load, as discussed in relation to OP3 and OP5 in Fig. 8 and Fig. 9. Note that the considered EGR calibration assumes reduced

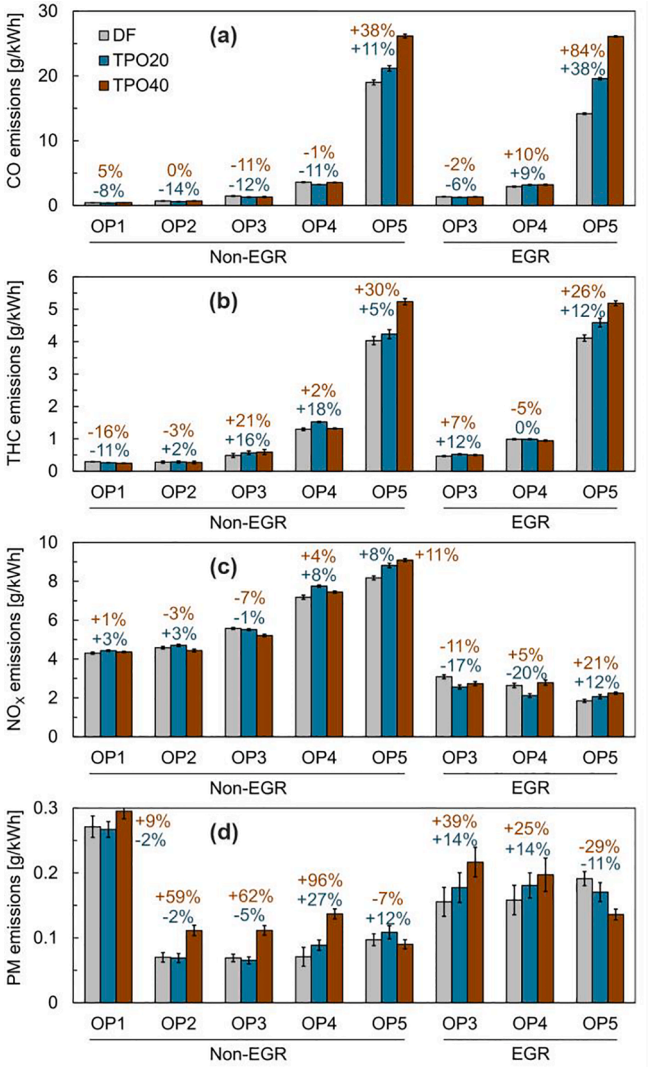

Fig. 11. Emissions of regulated compounds for the EGR and non-EGR calibration. Numbers above the individual bars denote the delta between respective TPO samples and DF as a reference.

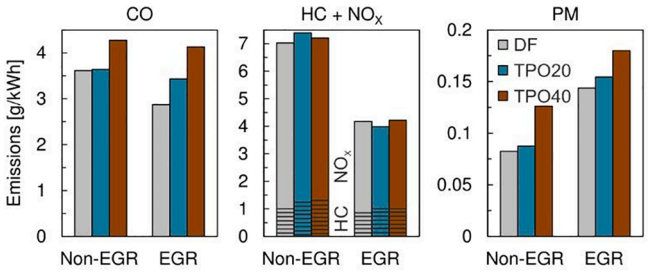

Fig. 12. Cycle-averaged emissions of regulated compounds calculated in accordance with ISO 8178 D2 stationary test.

recirculation rates with increasing load. Thus, the HRR at the mid-load OP3 with 10% and 0% EGR are nearly identical for respective fuels. Still, even 10% EGR influences the mixturés specific heat, therefore cutting combustion temperature while reducing oxygen concentration, substantially affecting thermal NO_X formation.

Fig. 10 extends the context of the above discussion for all operating points with the results of the single-most sensitive combustion indicator – the start of the high-temperature heat release of the pilot fuel (as

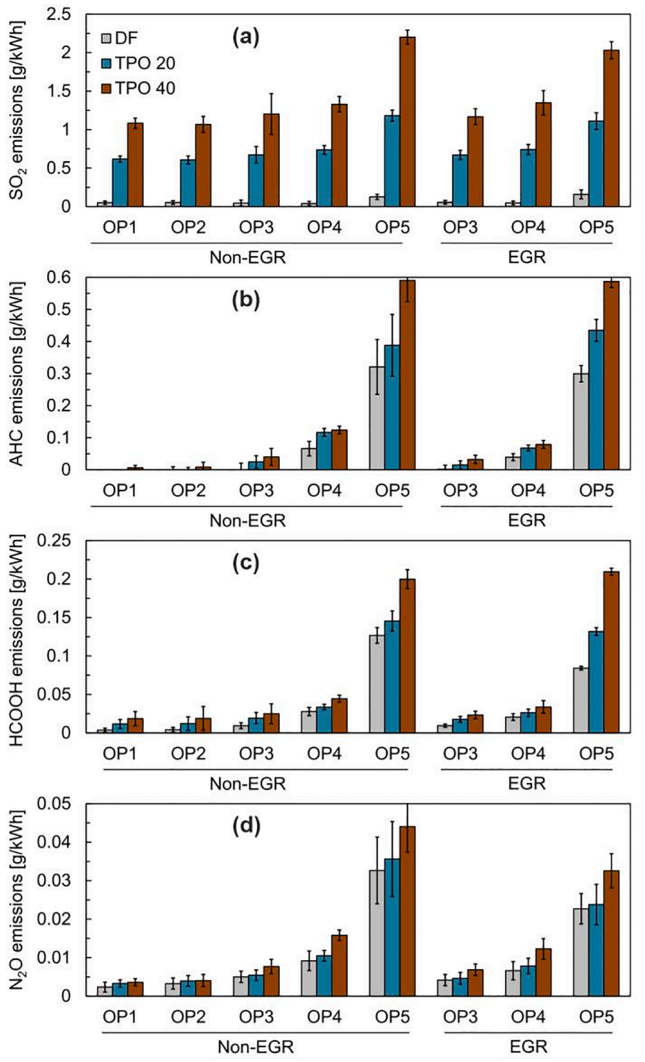

Fig. 13. Emissions of SO_2 (a); aromatic hydrocarbons (b); formic acid (c); and nitrous oxide (d) for the EGR and non-EGR calibrations.

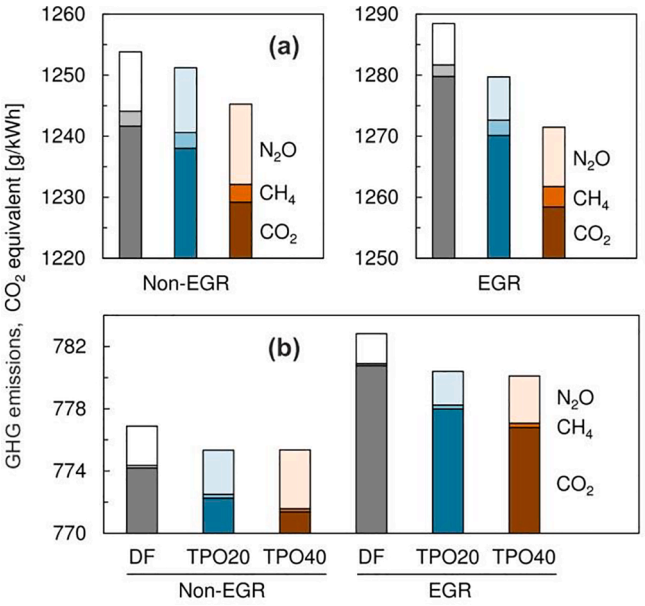

Fig. 14. Total brake-specific GHG emissions in grams of CO_2 equivalent for tested fuels for OP5 (a) and test cycle-averaged (b).

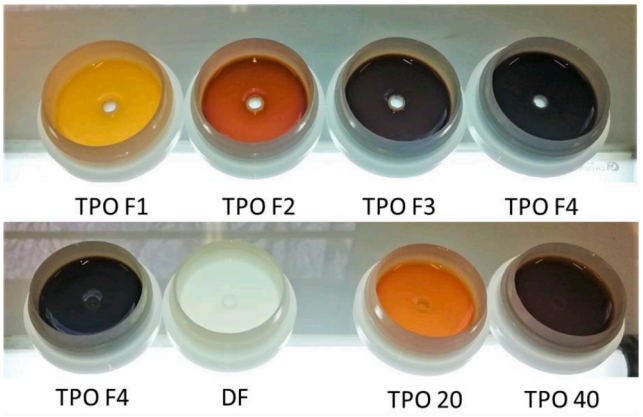

Fig. A1. Fractions obtained from the distillation of TPO Crude. Fraction TPO F4 has been used to create TPO20 and TPO40 – respectively 20% and 40% blends of TPO F4 with diesel, further used for engine tests.

indicated in Fig. 7). These summarizing results are provided as ignition delaay with respect to the start of pilot fuel injection (SOI_p) reference (Table 4). It is evident from Fig. 10 that TPO addition causes monotonically increased autoignition delay, however only at partial engine loads. Note, that uncertainty error bars presented here reflect the standard deviation from 300 cycles (100 cycles per individual OP, times 3 repetitions of the the test cycle). In this context, the maximum error of +-0.4 CA, along with a single-digit absolute value differences reported in Fig. 10 at OP5, allows concluding that the fuel to fuel differences in combustion characteristics, discussed earlier for Figs. 6-9 are statistically significant and repeatable.

Ultimately, we underline that overall high combustion stability both from cycle to cyle and from test to test is attributed to the pricece thermal conditioning of air and fuel paths provided by the SCRE test setup. Lowest repeatability (standard deviation in start of combustion between 0.6 and 0.9 CA depending on fuel) was observed at OP3, probably due to some injector histerisys at this particular setpoint. Note from Fig. 10, that there are no systematic differences in combustion stability between DF and TPO blends.

3.3. Regulated emissions

The combustion analysis gives context to the emission results presented in Fig. 11. As proven in the previous section, at elevated loads there are no significant differences in HRR between the tested fuels. Thus, any differences in emissions that manifest in OP1-OP3, can be attributed purely to the fuelś properties and chemical make-up, as listed in Table 5. In this load regime, TPO samples did not cause deterioration in any of the regulated emissions, except PM. Between OP1 and OP3 the fuel-to-fuel differences in emissions of CO, UHC and NO_X are within the limits of statistical relevance (note standard deviation levels in Fig. 11). It is therefore safe to conclude that the composition of the test samples does not affect the emissions of the above-mentioned species. The only effects are those originating from the combustion characteristics. In fact, these effects manifest only at the lowest load case (OP5), where the fuel quality effects on HRR are most pronounced (Fig. 5).

According to Fig. 11, at OP5, the lowest load point, the CO, UHC and NO_X emissions are increased for TPO40 by 38%, 30% and 11% respectively, compared to the non-EGR DF baselines. This low-load point is where the brake-specific emission results are globally the highest, attributable equally to physical effects and reduced brake efficiency. Note, that in the context of maximum error indicated in Fig. 11, the elevated emissions results obtained for TPO20 and TPO40 are repeatable. Comparing these OP5 emission results with the corresponding HRR

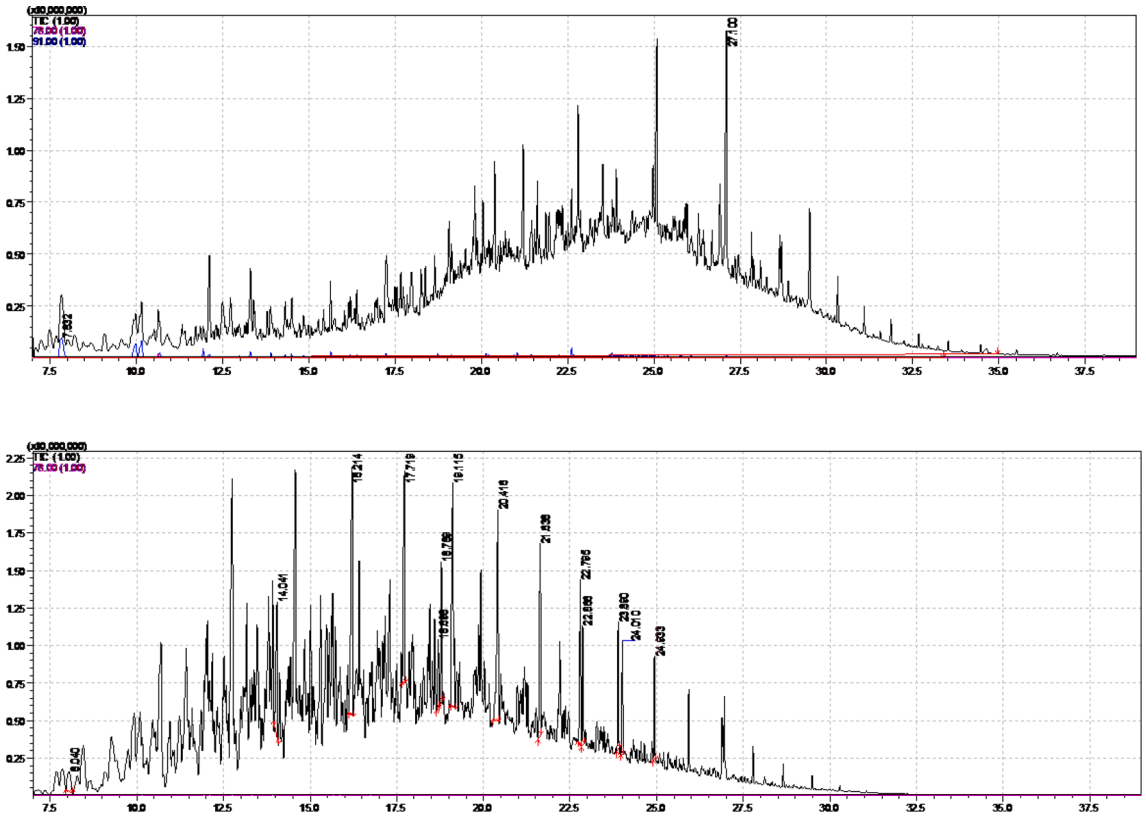

Fig. A2. Direct chromatogram from the GC–MS analysis of TPO F4 (upper plot) and DF (lower plot). Note that peak mass spectrometer counts for individual analytes are an order of magnitude lower for TPO F4 (upper plot). Compounds with very similar retention times give peaks overlapping each other, so their exact area cannot be calculated. This represents a particular challenge in determining individual hydrocarbon compounds in TPO. The content of hydrocarbons in this study was calculated on the basis of the area under the base curve of the chromatogram, within the limits determined as the retention times of the hydrocarbon reference standard.

Table A3
US Tier 4 emission standards for non-road applications. Engines up to 560 kW; emissions in g/kWh.

Engine Power	Year	CO	NMHC	NMHC + NO_x	NO_x	PM
kW < 8	2008	8.0	–	7.5	–	0.4[a]
8 ≤ kW < 19	2008	6.6	–	7.5	–	0.4
19 ≤ kW < 37	2008	5.5	–	7.5	–	0.3
	2013	5.5	–	4.7)	–	0.03
37 ≤ kW < 56	2008	5.0	–	4.7	–	0.3[b]
	2013	5.0	–	4.7	–	0.03
56 ≤ kW < 130	2012-2014[c]	5.0	0.19	–	0.40	0.02
130 ≤ kW ≤ 560	2011-2014[d]	3.5	0.19	–	0.40	0.02

Note that we have discussed the emission results in the context of the 2013 emission limit for engines in the 37 ≤ kW < 56 power range. This is based on the estimated power output from a conventional four-cylinder, small gen-set application of the given single-cylinder research engine.

[a] hand-startable, air-cooled, DI engines may be certified to Tier 2 standards through 2009 and to an optional PM standard of 0.6 g/kWh starting in 2010.

[b] 0.4 g/kWh (Tier 2) if the manufacturer complies with the 0.03 g/kWh standard from 2012.

[c] PM/CO: full compliance from 2012; NOx/UHC: Option 1 (if banked Tier 2 credits used)—50 % engines must comply in 2012–2013; Option 2 (if no Tier 2 credits claimed) 25% engines must comply in 2012–2014, with full compliance from 2014.12.31.

[d] PM/CO: full compliance from 2011; NOx/UHC: 50% engines must comply in 2011–2013.

traces in Fig. 6 provides a phenomenological explanation of the observed emission trends. As already discussed in the previous section, the increase in NO_X for higher TPO admixtures is caused by the reduction in CI shifting the combustion towards the main high-temperature phase. The elevated combustion temperatures for TPO translate directly into more NO_X formation. Increased UHC and especially CO originate from the fact that TPO combustion is delayed towards the expansion phase (see Fig. 6a) and thus, subjected to flame quenching when the piston is approaching exhaust valve opening.

The emissions results for the OP5-EGR case in Fig. 11 confirm the fuel-to-fuel trends for the non-EGR case, discussed above. Differences in emissions between TPO samples and DF become more pronounced as the CI-invoked combustion effects are intensified, though NO_X emission is generally reduced with EGR.

Fig. 11s PM emission results stand out from the trends exhibited by the other legislative compounds. Bearing in mind the measurement uncertainty, there is no particular fuel-related effect on PM when using 20% TPO admixture instead of the DF reference. However, use of the TPO40 shows a step increase in PM emissions across partial-load cases. PM is 96% higher versus DF at OP4. This suggests that PM formation is supported by greater amounts of contaminants - particularly sulphur - in the fuel. This issue, discussed in the introduction, is commonly reported in relation to TPO. There is a reversal of the situation at the lowest load, OP5, where TPO40s PM emissions are less than DFs. This is a manifestation of the combustion-related effects discussed earlier, whereby the higher peak HRR that is responsible for greater NOx production for TPO in OP5 also goes a long way in reducing the local λ -temperature regions that support PM formation. This is a typical manifestation of the known NO_X/PM dilemma.

At this point we can only speculate why TPO20 does not exhibit the

same behaviour in PM emissions as TPO40. On the one hand, the particulates tend to accumulate in the exhaust plenum, which carries a rather large maximum uncertainty of +/- 15% (refer to error bars on PM points in Fig. 11). Note, this is despite 20 min-backflush runs after each OP. This implies that PM emissions recorded for TPO20 that are lower than DF́s at some points should be regarded as statistically irrelevant. On the other hand, the TPO20 PM results seen in Fig. 11 exhibit the PM/NOx trade-off, implying that small-scale differences in combustion characteristics are overlapping with fuel quality effects.

The above discussion points are wrapped-up with Fig. 12, showing emission results averaged over the test cycle used for the US EPA Tier 4 emission limits for non-road engines (Appendix 3). One can note that any negative effect of TPO on UHC and NO_X emissions practically disappears over the whole test cycle. But the effect on CO emissions remains discernible, especially with EGR calibration, where TPO40́s result is 47% above the DF baseline. This is particularly due to TPÓs effect on the low-load cases, where OP5 brings the biggest net penalty and OP4 contributes with the highest weight to the cycle-averaged emissions. PM is obviously elevated for TPO due to the high contribution of partial-load cases. The key point to emerge from Fig. 12 is that a contemporary diesel engine with high-pressure EGR, operated on large-scale admixtures of TPO, can still meet the current Tier 4 emission limits without recalibration. Even without dedicated aftertreatment, this is true for combined UHC and NO_X emissions, where the Tier 4 limit for the representative engine category is 4.7 g/kWh. The same is true for CO, where the equivalent Tier 4 limit is 5 g/kWh. The elevated emissions of PM are less of a problem for TPO, bearing in mind that the engine would still require a particulate filter even while operating on ultra-low sulphur automotive diesel. Tier 4́s current PM emission limit for stationary gen-set applications is stringent: at 0.03 g/kWh it is an order of magnitude lower than the results presented here as the baseline. Note that Tier 4́s PM limit for engines produced before 2013 is 10 times higher, at 0.3 g/kWh. In this case, both DF and TPO40 could comply with this legacy emission norm with a decent margin. Appendix 3 provides more information on the relevent US Tier 4 emission legislation.

3.4. Unregulated emissions and tank-to-wheel greenhouse gas effect

As concluded in the earlier section, complying with emission legislation is not a major show-stopper for TPO fuels. On the other hand, polyaromatic emissions are widely highlighted in literature as a potential stumbling block for use of TPO. Until now, unregulated emissions from TPO have not been thoroughly studied. Fig. 13 presents the emissions results for four selected unregulated compounds relevent to a fueĺs environmental/health impacts. Note that we have displayed only compounds for which emissions are significantly fuel-dependent. The results presented are calculated as brake-specific, to correspond with emission test requirements. The clear increasing trend in all emission quantifiers while moving from OP1 to OP5 is primarily a manifestation of deteriorating brake efficiency as the load diminishes. On a mass basis, the emissions at lower loads are actually lower than at high loads, due to less fuel being burnt.

The sulphur dioxide (SO_2) emission results are directly related to sulphur content in the fuel samples, as listed in Table 5. This is evident in Fig. 13, where increasing the TPO content from 20% to 40% doubles the SO_2 footprint at every operating point. Bear in mind that the TPO used in these tests has not been subjected to any desulphurisation process, so, in principle, SO_2 emissions could be reduced by an order of magnitude. This would be necessary if the sulphur content limit was lowered from the current 0.6% to the 0.1% foreseen by the ISO 8127 standard for marine low-sulphur fuel oils. The lower limit is achievable for TPO, even with inexpensive non-refinery grade desulphurisation techniques [58].

Other emission quantifiers presented in Fig. 13 cannot be so easily removed by fuel pre-treatment. Aromatic hydrocarbon (AHC) emission is doubled for TPO40 compared to DF. TPO fuels are highly aromatic and some tailoring is possible, balancing hydrocarbon composition by being selective on feedstock [59], optimising pyrolysis process temperatures [60] or by accurate fractionation [61]. Emissions of aromatics higher than for DF simply needs to be acknowledged for TPO. The high content of polyaromatics in TPO, as discussed in section 3.1, is most probably transferred to the exhaust gas compositions and as such poses a challenge due to genotoxicity and carcinogenicity. Fuel-bound polyaromatics, as is the case with sulphur particles, are known to increase PM production in combustion engines [62], but the results seen in Fig. 11 suggest the PM mechanism is dominated by the combustion mode itself.

Fig. 13 also shows that formic acid (HCOOH) emissions increase with the level of TPO admixture. This is most probably due to TPÓs own carboxylic acid content. Despite the acidity being too small to cause any corrosive effects in fuel systems, as demonstrated by the copper-strip corrosion test results in Table 5, the fueĺs increased acidic content manifests as elevated HCOOH emissions in the exhaust. Besides its propensity to create teratogenic methanamide, when formic acid is entered into a reaction with other combustion products it is extremely corrosive, which may pose maintenance problems and poison catalytic converters [63]. Consequently, the acidity of TPO should be carefully considered when optimising the pyrolysis process. Note, however, that the influence of pyrolysis conditions on acidity has not been studied sufficiently in the literature [15].

The reasons for the elevated AHC, HCOOH and SO_2 emissions can be easily traced when looking at TPÓs molecular make-up. This study provides hard, quantitative proof and confirms anticipated issues related to TPO in engine applications that have been raised in the literature. However, Fig. 13́s final subplot, depicting N_2O, brings new knowledge. The current focus on GHG mitigation means emissions of other atmospheric heat absorbers, as well as CO_2, are being recognised as a potential climate threat. Aside from methane (CH_4), with 100-year global warming potential (GWP) of 36, the GWP of nitrous oxide (N_2O) is 310 times that of CO_2 for a 100-year timescale [64]. Fig. 13 reveals elevated N_2O emissions levels for TPO20 and TPO40 compared with the DF baseline. Some studies on marine fuels reported N_2O formation correlated with SO_2 emissions [65]. This correlation is seen in Fig. 13, and it is plausible to assume that TPÓs elevated N_2O emissions are attributable to fuel-bound sulphur. The mechanisms of these effects are ultimately not well researched and require more fundamental studies.

Fig. 14 presents the N_2O contribution to the total tank-to-wheel GHG emissions of the tested fuel samples. For clarity, this is narrowed down to the most-contributing OP5 point and test cycle- averaged results. It is worth noting, that N_2O levels from contemporary diesel engines, as represented by the one used in this research, are an order of magnitude higher than from their legacy predecessors. due to the combustion concept focusing on NO_X mitigation [66]. Specifically, lower local combustion temperatures do not support the complete oxidation of NO particles that tend to follow the low-temperature N_2O formation pathways. Fig. 14 shows that N_2Ós contribution to the total GHG emissions from TPO40 samples is significant, being around 13.5 g/kWh of CO_2 equivalent at low-load OP5. Ultimately, N_2O is responsible for 1.1% of the total GHG emission of TPO40 at this operating point. The corresponding proportion for DF is 0.8%. Note, that aside from the radiative absorption effect described by the GWP factor, migration of N_2O to the stratosphere contributes to ozone layer destruction [67].

The fuel-to-fuel differences in total GHG emissions across the whole test cycle are minor, with those from both TPO samples roughly 0.3% lower than DF́s GHG emissions for the EGR calibration. The slightly lower CO_2 output from the TPO blends compared to DF is attributed mainly to TPÓs elevated CO emissions (revert to Fig. 11), as both fuels have a similar molecular carbon to hydrogen ratio.

4. Conclusions and outlook

This study provides the first comprehensive analysis of industry-grade, TPO-derived fuels in state-of-the-art compression ignition

engines. It draws the following conclusions:.

1. It is currently possible to produce high-quality crude TPO on an industrial scale, while keeping the installation economically feasible. The end product is characterised by low sulphur content of 0.5% and acceptable acidity, making it suitable as low-sulphur fuel oil for marine applications.
2. Fractionation and blending allow for inexpensive fuel mixtures that meet stringent automotive fuel standards in all parameters except sulphur content. Still, fuel with up to 40% of heavy TPO fraction is appropriate for contemporary compression ignition engines in genset applications.
3. Tier 4-compliant combustion systems with multi-pulse injection can handle high TPO-content fuels without needing re-calibration. For 40% TPO admixture to diesel, the combustion is significantly delayed (by 3 CAD) only at low engine-loads, particularly with the use of heavy exhaust gas recirculation. This impacts UHC and CO emissions, which are increased by 26% and 84% respectively in this regime.
4. While the above can be easily mitigated by re-calibration, the differences in UHC and NO_X practically disappear over the full test cycle, due to the highly weighted contribution of higher load points, which remain insensitive to TPO. Test-cycle CO emissions for the 40% TPO admixture remain elevated by 21% and 45% for the non-EGR and EGR calibrations respectively.
5. PM emissions from the 40% TPO admixture are up to 25% higher than the diesel baseline. This is attributed primarily to fuel-bound sulphur and contamination, rather than the combustion process, and must be acknowledged.
6. Despite the above-mentioned issues, the current EPA Tier 4 emission limits are not a particular challenge for TPO, even for the 40% blending rate. However, the elevated unregulated emissions should be considered in total environmental impact.
7. Regardless of calibration, TPO mixtures emit substantially more sulphur oxides, aromatics, and formic acid, presenting health concerns and maintenance problems. The increase in emissions of those species correlates directly with fuel sulphur content, polyaromatic hydrocarbon structure and acidity.
8. Elevated nitrous oxide and methane emissions from TPO combustion add 5 g/kWh of CO_2 equivalent GHG emissions for the 40% TPO mixture, versus 2.5 g/kWh for the diesel baseline. This is still minor in terms of the fuel's tank-to-wheel greenhouse gas emissions and does not jeopardise TPO's carbon footprint advantage as waste-derived fuel.

As the outlook, one can consider two pathways to improve the contemporary situation discussed here. Specific engine calibration for TPO mixtures offers minor improvement, predominantly to carbon monoxide emissions and thermal efficiency/CO_2 emissions. However, the primary improvement route still entails optimising TPÓs composition. This can be done at the reactor level and via improved fuel post-processing. Sulphur content and acidity in particular can still be reduced, as both are responsible for the majority of unregulated emissions.

CRediT authorship contribution statement

Maciej Mikulski: Conceptualization, Methodology, Investigation, Validation, Writing – original draft, Writing – review & editing, Project administration, Supervision. **Jacek Hunicz:** Conceptualization, Methodology, Investigation, Formal analysis, Visualization, Resources, Writing – original draft, Writing – review & editing, Funding acquisition. **Kamil Duda:** Methodology, Investigation, Resources, Writing – original draft. **Paweł Kazimierski:** Methodology, Investigation, Resources, Writing – original draft. **Tomasz Suchocki:** Methodology, Investigation, Resources, Writing – original draft. **Arkadiusz Rybak:** Data curation, Software, Writing – review & editing, Visualization.

Declaration of Competing Interest

The authors declare that they have no known competing financial interests or personal relationships that could have appeared to influence the work reported in this paper.

Acknowledgements

The research was financed in the framework of the project Lublin University of Technology, Regional Excellence Initiative, funded by the Polish Ministry of Science and Higher Education (contract No. 030/RID/2018/19).

The authors wish to thank AVL List GmbH for making the simulation software available within a framework of the AVL University Partnership Program.

Appendix 1. .

(See Fig. A1).

Appendix 2. .

(See Fig. A2).

Appendix 3. .

(See Table A3).

References

[1] Reitz RD, Ogawa H, Payri R, Fansler T, Kokjohn S, Moriyoshi Y, et al. The future of the internal combustion engine. Int J Engine Res 2019;21:3–10. https://doi.org/10.1177/1468087419877990.
[2] Energy demand: Three drivers | ExxonMobil n.d. https://corporate.exxonmobil.com/Energy-and-innovation/outlook-for-energy/Energy-demand#Threedriversofenergydemand (accessed January 6, 2022).
[3] Worldwide Emission Standards and Related Regulations 2019. www.continental-automotive.comPowertrain (accessed January 6, 2022).
[4] Vignesh P, Pradeep Kumar AR, Shankar Ganesh N, Jayaseelan V, Sudhakar K. A review of conventional and renewable biodiesel production. Chinese J Chem Eng 2021;40:1–17.
[5] Duda K, Wierzbicki S, Śmieja M, Mikulski M. Comparison of performance and emissions of a CRDI diesel engine fuelled with biodiesel of different origin. Fuel 2018;212:202–22. https://doi.org/10.1016/J.FUEL.2017.09.112.
[6] Shukla PC, Gupta T, Labhsetwar NK, Agarwal AK. Physico-chemical speciation of particulates emanating from Karanja biodiesel fuelled automotive engine. Fuel 2015;162:84–90. https://doi.org/10.1016/J.FUEL.2015.07.076.
[7] Neste Renewable Diesel Handbook n.d. https://www.neste.com/sites/default/files/attachments/neste_renewable_diesel_handbook.pdf (accessed January 6, 2022).
[8] Di Blasio G, Ianniello R, Beatrice C. Hydrotreated vegetable oil as enabler for high-efficient and ultra-low emission vehicles in the view of 2030 targets. Fuel 2022;310:122206.
[9] Mikulski M, Vasudev A, Hunicz J, Rybak A, Gęca M. Combustion of hydrotreated vegetable oil in a diesel engine: Sensitivity to split injection strategy and exhaust gas recirculation. In: ASME 2020 Intern Combust Engine Div Fall Tech Conf ICEF; 2021. https://doi.org/10.1115/ICEF2020-2936.
[10] Hunicz J, Mikulski M, Shukla PC, Gęca MichałS. Partially premixed combustion of hydrotreated vegetable oil in a diesel engine: Sensitivity to boost and exhaust gas recirculation. Fuel 2022;307:121910.
[11] Energy Outlook 2020 edition n.d. https://www.bp.com/content/dam/bp/business-sites/en/global/corporate/pdfs/energy-economics/energy-outlook/bp-energy-outlook-2020.pdf (accessed January 6, 2022).
[12] Torretta V, Rada EC, Ragazzi M, Trulli E, Istrate IA, Cioca LI. Treatment and disposal of tyres: Two EU approaches. A review Waste Manag 2015;45:152–60. https://doi.org/10.1016/J.WASMAN.2015.04.018.
[13] Hita I, Arabiourrutia M, Olazar M, Bilbao J, Arandes JM, Castaño SánchezP. Opportunities and barriers for producing high quality fuels from the pyrolysis of scrap tires. Renew Sustain Energy Rev 2016;56:745–59. https://doi.org/10.1016/J.RSER.2015.11.081.
[14] Antoniou N, Zabaniotou A. Features of an efficient and environmentally attractive used tyres pyrolysis with energy and material recovery. Renew Sustain Energy Rev 2013;20:539–58. https://doi.org/10.1016/J.RSER.2012.12.005.

[15] Mikulski M, Ambrosewicz-Walacik M, Hunicz J, Nitkiewicz S. Combustion engine applications of waste tyre pyrolytic oil. Prog Energy Combust Sci 2021;85:100915.
[16] Chen R, Lun L, Cong K, Li Q, Zhang Y. Insights into pyrolysis and co-pyrolysis of tobacco stalk and scrap tire: Thermochemical behaviors, kinetics, and evolved gas analysis. Energy 2019;183:25–34. https://doi.org/10.1016/J.ENERGY.2019.06.127.
[17] Zhao XY, Ren J, Cao JP, Wei F, Zhu C, Fan X, et al. Catalytic Reforming of Volatiles from Biomass Pyrolysis for Hydrogen-Rich Gas Production over Limonite Ore. Energy Fuels 2017;31:4054–60. https://doi.org/10.1021/ACS.ENERGYFUELS.7B00005/SUPPL_FILE/EF7B00005_SI_001.PDF.
[18] Hopa DY, Yilmaz A, Bahtli TA. Recovery of waste tyres by pyrolysis in a fixed bed reactor for liquid fuel production: effects of pyrolysis conditions on oil yield. Res Eng Struct Mater 2017. https://doi.org/10.17515/resm201510.17515/resm2016.58en0701.
[19] Aylón E, Fernández-Colino A, Murillo R, Navarro MV, García T, Mastral AM. Valorisation of waste tyre by pyrolysis in a moving bed reactor. Waste Manag 2010;30(7):1220–4.
[20] Ayanoğlu A, Yumrutaş R. Production of gasoline and diesel like fuels from waste tire oil by using catalytic pyrolysis. Energy 2016;103:456–68. https://doi.org/10.1016/J.ENERGY.2016.02.155.
[21] Xu J, Yu J, He W, Huang J, Xu J, Li G. Recovery of carbon black from waste tire in continuous commercial rotary kiln pyrolysis reactor. Sci Total Environ 2021;772:145507.
[22] Khan MZH, Hossain MI, Halder PK, Hasan MR, Al-Mamun MR. Fuel properties of pyrolytic tyre oil and its blends with diesel fuel - Towards waste management. Int J Environ Waste Manag 2016;18:335–48. https://doi.org/10.1504/IJEWM.2016.081835.
[23] Doğan O, Elik MB, Özdalyan B. The effect of tire derived fuel/diesel fuel blends utilization on diesel engine performance and emissions. Fuel 2012;95:340–6. https://doi.org/10.1016/J.FUEL.2011.12.033.
[24] Yaqoob H, Teoh YH, Jamil MA, Gulzar M. Potential of tire pyrolysis oil as an alternate fuel for diesel engines: A review. J Energy Inst 2021;96:205–21. https://doi.org/10.1016/J.JOEI.2021.03.002.
[25] Galvagno S, Casu S, Casabianca T, Calabrese A, Cornacchia G. Pyrolysis process for the treatment of scrap tyres: preliminary experimental results. Waste Manag 2002;22(8):917–23. https://doi.org/10.1016/S0956-053X(02)00083-1.
[26] Chiong M-C, Kang H-S, Shaharuddin NMR, Mat S, Quen LK, Ten K-H, et al. Challenges and opportunities of marine propulsion with alternative fuels. Renew Sustain Energy Rev 2021;149:111397.
[27] Al-Lal AM, Bolonio D, Llamas A, Lapuerta M, Canoira L. Desulfurization of pyrolysis fuels obtained from waste: Lube oils, tires and plastics. Fuel 2015;150:208–16. https://doi.org/10.1016/J.FUEL.2015.02.034.
[28] Aydin H, Ilkiliç C. Optimization of fuel production from waste vehicle tires by pyrolysis and resembling to diesel fuel by various desulfurization methods. Fuel 2012;102:605–12. https://doi.org/10.1016/J.FUEL.2012.06.067.
[29] Mikulski M, Ambrosewicz-Walacik M, Duda K, Hunicz J. Performance and emission characterization of a common-rail compression-ignition engine fuelled with ternary mixtures of rapeseed oil, pyrolytic oil and diesel. Renew Energy 2020;148:739–55. https://doi.org/10.1016/J.RENENE.2019.10.161.
[30] Hunicz J, Beidl C, Knost F, Münz M, Runkel Jürgen, Mikulski M. Injection Strategy and EGR Optimization on a Viscosity-Improved Vegetable Oil Blend Suitable for Modern Compression Ignition Engines. SAE Tech Pap 2021;3(1):419–27. https://doi.org/10.4271/2020-01-2141.
[31] Żółtowski A. Tyre pyrolysis oil as an engine fuel. J KONES Powertrain Transp 2014;21(1):295–302. https://doi.org/10.5604/12314005.1134118.
[32] Vihar R, Seljak T, Rodman Oprešnik S, Katrašnik T. Combustion characteristics of tire pyrolysis oil in turbo charged compression ignition engine. Fuel 2015;150:226–35. https://doi.org/10.1016/J.FUEL.2015.01.087.
[33] Sharma A, Murugan S. Investigation on the behaviour of a DI diesel engine fueled with Jatropha Methyl Ester (JME) and Tyre Pyrolysis Oil (TPO) blends. Fuel 2013;108:699–708. https://doi.org/10.1016/J.FUEL.2012.12.042.
[34] Martínez JD, Rodríguez-Fernández J, Sánchez-Valdepeñas J, Murillo R, García T. Performance and emissions of an automotive diesel engine using a tire pyrolysis liquid blend. Fuel 2014;115:490–9. https://doi.org/10.1016/J.FUEL.2013.07.051.
[35] Murugan S, Ramaswamy MC, Nagarajan G. Performance, emission and combustion studies of a DI diesel engine using Distilled Tyre pyrolysis oil-diesel blends. Fuel Process Technol 2008;89(2):152–9.
[36] Hossain FM, Nabi MN, Rainey TJ, Bodisco T, Bayley T, Randall D, et al. Novel biofuels derived from waste tyres and their effects on reducing oxides of nitrogen and particulate matter emissions. J Clean Prod 2020;242:118463.
[37] Verma P, Zare A, Jafari M, Bodisco TA, Rainey T, Ristovski ZD, et al. Diesel engine performance and emissions with fuels derived from waste tyres. Sci Reports 2018.1–13.;2018(81):8. https://doi.org/10.1038/s41598-018-19330-0.
[38] Vihar R, Žvar Baškovič U, Seljak T, Katrašnik T. Combustion and emission formation phenomena of tire pyrolysis oil in a common rail Diesel engine. Energy Convers Manag 2017;149:706–21. https://doi.org/10.1016/J.ENCONMAN.2017.02.005.
[39] Hunicz J, Matijošius J, Rimkus A, Kilikevičius A, Kordos P, Mikulski M. Efficient hydrotreated vegetable oil combustion under partially premixed conditions with heavy exhaust gas recirculation. Fuel 2020;268:117350.
[40] Williams PT, Bottrill RP, Cunliffe AM. Combustion of Tyre Pyrolysis Oil. Process Saf Environ Prot 1998;76(4):291–301. https://doi.org/10.1205/095758298529650.
[41] Johansson A-C, Molinder R, Vikström T, Wiinikka H. Particle formation during suspension combustion of different biomass powders and their fast pyrolysis bio-oils and biochars. Fuel Process Technol 2021;218:106868.
[42] Bae HR, Chandy M, Aguilera J, Smith EM, Nadeau KC, Wu JC, et al. Adverse effects of air pollution-derived fine particulate matter on cardiovascular homeostasis and disease. Trends Cardiovasc Med 2021.
[43] He C, Li J, Wang Y, Tan J, Song G, Jia D, et al. Size-segregated particulate matter emission characteristics of a heavy-duty diesel engine with oxygenated fuels. Appl Therm Eng 2017;125:1173–80.
[44] Žvar Baškovič U, Vihar R, Seljak T, Katrašnik T. Feasibility analysis of 100% tire pyrolysis oil in a common rail Diesel engine. Energy 2017;137:980–90. https://doi.org/10.1016/J.ENERGY.2017.01.156.
[45] Palos R, Rodríguez E, Gutiérrez A, Bilbao J, Arandes JoséM. Kinetic modeling for the catalytic cracking of tires pyrolysis oil. Fuel 2022;309:122055.
[46] Teoh YH, Yaqoob H, How HG, Le TD, Nguyen HT. Comparative assessment of performance, emissions and combustion characteristics of tire pyrolysis oil-diesel and biodiesel-diesel blends in a common-rail direct injection engine. Fuel 2022;313:123058.
[47] Duda K, Kazimierski P, Suchocki T, Rybak A, Hunicz J, Mikulski M. Tailored blending strategies for tyre pyrolytic oil – derived engine fuels. Prep 2022.
[48] Kasprzyk P, Hunicz J, Rybak A, Gęca MS, Mikulski M. Excess Air Ratio Management in a Diesel Engine with Exhaust Backpressure Compensation. Sensors; 2020, Vol 20, Page 6701 2020;20:6701. Doi: 10.3390/S20226701.
[49] Mikulski M, Wierzbicki S. Validation of a zero-dimensional and two-phase combustion model for dual-fuel compression ignition engine simulation. Therm Sci 2017;21:387–99. https://doi.org/10.2298/TSCI160127076M.
[50] Hohenberg GF. Advanced approaches for heat transfer calculations. SAE Tech Pap 1979. https://doi.org/10.4271/790825.
[51] Kline S, McClintock F. Describing Uncertainty in Single Sample Experiments. Mech Eng 1953;75:3–8.
[52] Mikulski M, Duda K, Wierzbicki S. Performance and emissions of a CRDI diesel engine fuelled with swine lard methyl esters–diesel mixture. Fuel 2016;164:206–19.
[53] Csemány Dávid, DarAli O, Rizvi SAH, Józsa V. Comparison of volatility characteristics and temperature-dependent density, surface tension, and kinematic viscosity of n-butanol-diesel and ABE-diesel fuel blends. Fuel 2022;312:122909.
[54] Alvarez J, Lopez G, Amutio M, Mkhize NM, Danon B, van der Gryp P, et al. Evaluation of the properties of tyre pyrolysis oils obtained in a conical spouted bed reactor. Energy 2017;128:463–74.
[55] Cormier SA, Lomnicki S, Backes W, Dellinger B. Origin and health impacts of emissions of toxic by-products and fine particles from combustion and thermal treatment of hazardous wastes and materials. Environ Health Perspect 2006;114(6):810–7.
[56] IMO 2020 – cutting sulphur oxide emissions n.d. https://www.imo.org/en/MediaCentre/HotTopics/Pages/Sulphur-2020.aspx (accessed January 6, 2022).
[57] Emission Standards: USA: Nonroad Diesel Engines n.d. https://dieselnet.com/standards/us/nonroad.php#tier3 (accessed January 6, 2022).
[58] Yasar A, Rana S, Moniruzzaman M, Nazar M, Tabinda AB, Haider R, et al. Quality and environmental impacts of oil production through pyrolysis of waste tyres. Environ Technol Innov 2021;23:101565.
[59] Kumar Singh R, Ruj B, Jana A, Mondal S, Jana B, Kumar Sadhukhan A, et al. Pyrolysis of three different categories of automotive tyre wastes: Product yield analysis and characterization. J Anal Appl Pyrolysis 2018;135:379–89.
[60] Díez C, Martínez O, Calvo LF, Cara J, Morán A. Pyrolysis of tyres. Influence of the final temperature of the process on emissions and the calorific value of the products recovered. Waste Manag 2004;24(5):463–9.
[61] Campuzano F, Abdul Jameel AG, Zhang W, Emwas A-H, Agudelo AndrésF, Martínez JD, et al. On the distillation of waste tire pyrolysis oil: A structural characterization of the derived fractions. Fuel 2021;290:120041.
[62] Furuhata T, Kobayashi Y, Hayashida K, Arai M. Behavior of PAHs and PM in a diffusion flame of paraffin fuels. Fuel 2012;91(1):16–25.
[63] Nova I, Tronconi E. Urea-SCR Technology for deNOx After Treatment of Diesel Exhausts. New York: Springer; 2014.
[64] Leitner S, Ring Dónal, Wanyama GN, Korir D, Pelster DE, Goopy JP, et al. Effect of feeding practices and manure quality on CH4 and N2O emissions from uncovered cattle manure heaps in Kenya. Waste Manag 2021;126:209–20.
[65] Sudrajad A. Nitrous Oxide Emissions on Single Cylinder Diesel Engine Using Variable of Fuel Sulfur and Emulsion Fuel. Int J Appl Eng Res 2017;12:7920–6.
[66] Clairotte M, Suarez-Bertoa R, Zardini AA, Giechaskiel B, Pavlovic J, Valverde V, et al. Exhaust emission factors of greenhouse gases (GHGs) from European road vehicles. Environ Sci Eur 2020;32:1–20. https://doi.org/10.1186/S12302-020-00407-5/FIGURES/8.
[67] Prigent M, De Soete G. Nitrous oxide N2O in engines exhaust gases-A first appraisal of catalyst impact. SAE Tech Pap 1989. https://doi.org/10.4271/890492.